CHINESE OPTICS LETTERS

Vol. 22, No. 3 | March 2024

Vortex localization and OAM selective conversion via cylindrical metagratings

Zhanlei Hao (郝占磊)[1,2], Shan Zhu (朱 杉)[1], Cheng-Wei Qiu (仇成伟)[2*], Yadong Xu (徐亚东)[3**], and Huanyang Chen (陈焕阳)[1***]

[1] Institute of Electromagnetics and Acoustics and Department of Physics, College of Physical Science and Technology, Xiamen University, Xiamen 361005, China

[2] Department of Electrical and Computer Engineering, National University of Singapore, Singapore 117583, Singapore

[3] School of Physical Science and Technology and Jiangsu Key Laboratory of Thin Films, Soochow University, Suzhou 215006, China

*Corresponding author: chengwei.qiu@nus.edu.sg

**Corresponding author: ydxu@suda.edu.cn

***Corresponding author: kenyon@xmu.edu.cn

Received September 2, 2022 | Accepted November 15, 2023 | Posted Online March 4, 2024

Vortex waves with orbital angular momentum (OAM) are a highly active research topic in various fields. In this paper, we design and investigate cylindrical metagratings (CMs) with an even number of unit cells that can efficiently achieve vortex localization and specific OAM selective conversion. The multifunctional manipulation of vortex waves and the new OAM conservation law have further been confirmed through analytical calculations and numerical simulations. In addition, we qualitatively and quantitatively determine the OAM range for vortex localization and the OAM value of vortex selective conversion and also explore the stability for performance and potential applications of the designed structure. This work holds potential applications in particle manipulation and optical communication.

Keywords: vortex waves; cylindrical metagratings; vortex localization; high-efficiency transmission; vortex selective conversion.

DOI: 10.3788/COL202422.033601

1. Introduction

The vortex is one of the most evident manifestations of orbital angular momentum (OAM) in nature, which is characterized by a helical phase-front and a ring-shaped intensity distribution[1,2]. In 1989, Coullet *et al.* introduced the concept of optical vortices in the framework of the Maxwell–Bloch model[3], and Allen *et al.* first demonstrated OAM in vortex beams with nonparaxial approximation propagating[4]. As our understanding and discussion of optical vortex deepens[5,6], various applications have also been gradually developed, including but not limited to wave manipulation[7,8], superresolution imaging[9–11], holography[12,13], and quantum information processing[14,15]. In particular, tremendous progress has been made in metamaterials and metasurfaces in recent years[16–18], pushing the development of OAM-based applications and devices to new heights, such as OAM efficient generation[19–21], utilizing whispering-gallery modes to achieve theoretical verification of optical OAM[22,23], OAM multiplexing and demultiplexing[24], and the spin-to-OAM conversion[25]. Therefore, OAM induces revolutionary developments in many research fields.

Although the vortex wave is ubiquitous and its importance is self-evident, the arbitrary OAM manipulation of the two-dimensional (2D) vortex wave remains largely unexplored. Phase-gradient metasurfaces (PGMs) have been repeatedly demonstrated to enable free manipulation of the propagation behavior of light waves and sound waves[26,27]. The PGMs composed of periodically arranged m supercells have the powerful advantages of high efficiency, small volume, thinness, and strong operability, and it has been proved that they can easily achieve anomalous transmission and reflection[28,29], asymmetric transmission[30–32], retroreflection[33], photonic spin Hall effect[34,35], perfect absorption[36], and other anomalous wave phenomena[37,38]. Inspired by the important role of the odd/even unit cells in the anomalous diffraction phenomenon of planar PGMs[28,30], it is a feasible and effective approach to achieve special manipulation of vortex waves. Many effective proposals have been previously proposed to achieve the OAM manipulation of optical or acoustic vortex waves, including chiral nanostructures[39], nonlinearity[40], non-Hermitian systems[41], and metasurfaces[42–45]. However, the previous reports have been limited by the low efficiency of vortex conversion and the lack

of the fundamental OAM conversion rules (such as the fact that vortex has a large OAM), which hinder the applicability of vortex waves in various scenarios.

In this work, we design a 2D cylindrical metagrating (CM) with m being even numbers, by analogy with the planar PGMs, and find that it can achieve vortex localization and specific OAM selective conversion. Due to the incorporation of periodic gradient refractive index materials in CMs, the additional structural topological charge enables the reflected and transmitted vortex waves to satisfy a new OAM conservation law. This work is based on the parity-dependent diffraction law in CMs to achieve the multifunctional control of vortex waves, and the proposed OAM conservation law is further confirmed by the analytical and numerical results. Finally, we quantitatively determine the OAM range of vortex localization and the OAM value of vortex selective conversion and explore stability performance and potential applications of the designed structure. For the stability of performance, the effects of wideband properties, off-center properties, and variations of the unit cell m are evaluated. For potential applications, the aspects of multi-vortex source localization and the selection of vortex waves with specific OAM are also considered. Notably, although the scheme was designed in the optical field, the concepts are expected to be extended to other physical fields, such as acoustic waves and water waves.

2. Results and Discussions

Figure 1(a) shows the schematic diagram of the multifunctional CMs. The designed ring-shaped structure is composed of N periodically repeated fanlike supercells; its inner radius is R_0. The period length and thickness of each supercell are p and d, respectively. Each supercell is divided equally into m unit cells, i.e., cell-1, cell-2, ..., cell-m, and the width of a unit cell is $a = p/m$. These unit cells consist of metallic slits with a width w (gray area), filled with a dielectric medium of different refractive indices (blue area). To obtain a 2π phase coverage over each supercell, the phase difference between adjacent unit cells should be $\Delta\phi = 2\pi/m$, which is achieved by applying the following index profile, i.e., $\varepsilon_j = \mu_j = 1 + (j-1)\lambda/md$, where $j = 1, 2, \ldots, m$, and λ is the working wavelength in air. In this way, the phase gradient of $\xi = 2\pi/p = \gamma k_0$ is introduced along azimuthal direction at the outer interface of $r = R_0 + d$, and the period length is $p = 2\pi/\xi$, where $k_0 = 2\pi/\lambda$ is the wavenumber in air, and γ is a number. The azimuthal phase gradient introduces additionally extrinsic topological charge, i.e., $q = \xi r = N$, for efficiently controlling the OAM of the vortex. According to the parity-dependent diffraction law in planar PGMs[28,30,31], similar diffraction behavior of OAM in CMs can be obtained by analogy with their planar counterpart[42]. To be specific, if considering an incident OAM source with l_{in} located at the center and diffracted by CMs, the OAM of transmission and refection vortex waves is ruled by

$$l_{r/t} = l_{\text{in}} + \sigma q, \tag{1}$$

where σ is the diffraction order, and r (t) indicates the reflection (transmission).

Equation (1) demonstrates the linear relationship between the reflected and transmitted OAMs and the incident OAM l_{in}, which are determined by σ and q. Figure 1(b) displays the physical process of two special vortex effects in CMs with m being even numbers. To quantitatively determine the range of OAM for vortex localization, further exploration about the critical OAM value of vortex localization is still needed. Considering that the designed structures are formed by rolling up the planar PGMs end to end, the introduction of curvature makes its diffraction behavior similar to, yet different from planar PGMs. For the transmission-type planar PGMs, the diffraction behavior of plane waves is governed by the following equation[28,30]:

$$k_0 \sin\theta_i = k_0 \sin\theta_{r/t} - \sigma\xi, \tag{2}$$

where θ_i is the incident angle, and $\theta_{r/t}$ is the reflection (refraction) angle. The physical meaning of OAM is the rotational equivalent of the parallel wave vector $k_{\parallel}$ of the plane wave, i.e., $k_{\parallel} R_0 = l$. Thus, multiplying both sides of Eq. (2) by R_0 yields the OAM conversion rule, as shown by Eq. (1). In addition, Eq. (1) indicates a critical incident angle that indicates the diffraction order transition, as does Eq. (2). Based on the diffraction results in planar PGMs presented in Refs. [27,28,30], the critical OAM indicating the diffraction order transition from $\sigma = 0$ to $|\sigma| = 1$ is given by (for more details see Ref. [42])

$$l_{\text{crt}} = q(\gamma - 1)/\gamma + \tau(\lambda, d), \tag{3}$$

where q is the topological charge introduced by CMs, and $\tau(\lambda, d)$ is the correction term introduced after the curvature R_0 is considered. According to the analytical results (details shown in Supplementary Material), the numerical fitting result is $\tau(\lambda, d) = -(k_0 d + \pi)$, which is physically interpreted as the phase compensation brought by vortex wave passing through CMs with thickness d. In contrast to the previously proposed metacages[46,47], the outstanding advantages of our approach are the stable functional performance and the high efficiency in both transmission and reflection. The different diffraction orders play a crucial role in the transmission or reflection

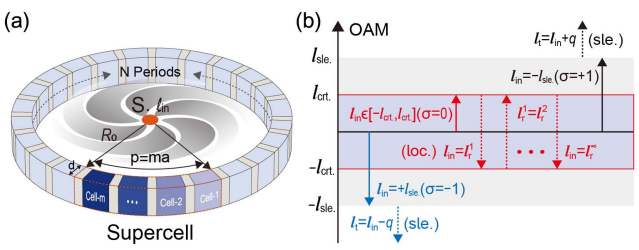

Fig. 1. (a) Schematic diagram of designed multifunctional CMs; (b) physics process of vortex localization and OAM selective conversion for all diffraction orders, where the solid (dashed) arrow denotes an incident vortex wave (reflected and transmitted vortex waves).

phenomena in the CMs. For the OAM of vortex sources below the critical OAM (where the critical OAM is equal to 0), the incident vortex wave will couple to the transmission channel of the $\sigma = 1$ order, independent of m. Beyond the critical OAM, the parity of the propagation number L completely determines the diffraction behavior of CMs, which is jointly modulated by the number of unit cells m and the diffraction order σ, satisfying $L = m + \sigma$. Specifically, when $l_{\text{in}} \in [-l_{\text{crt}}, l_{\text{crt}}]$, the $\sigma = 0$ diffraction channel is available and the diffraction wave takes the reflection channel, resulting in the function of vortex localization. Otherwise, the $\sigma = -1$ diffraction channel is open and it takes the transmission channel, contributing to the effect of vortex OAM selective conversion. For instance, the incident vortex wave with $|l_{\text{in}}| \approx q/2$ for $\gamma = 2$ will be accurately picked out and converted following Eq. (1), which exemplifies the phenomenon of selective conversion of vortex wave in CMs [shown by the blue and black arrows in Fig. 1(b)].

To illustrate the theoretical prediction for the multifunctional manipulation of vortex waves, we perform numerical simulations with COMSOL Multiphysics. The designed structure contains 20 supercells, each of which consists of 4 unit cells with the phase gradient arranged counterclockwise. In the numerical simulations, we utilize the $H^{(1)}_{l_{\text{in}}}(\cdot)e^{il_{\text{in}}\theta}$ to simulate 2D vortex fields. $H^{(1)}_{l_{\text{in}}}(\cdot)$ represents the l_{in}th order Hankel function of the first kind, which represents the vortex wave propagating outward from the center. The obtained numerical results are shown in Figs. 2(a)–2(d), respectively. For the effect of vortex localization, when the vortex wave with $l_{\text{in}} = 0$ or 5 is placed at the structural center, two different vortices are both perfectly confined inside the CMs, as shown in Figs. 2(a) and 2(b), respectively. The reflectivity of two cases calculated numerically is 98.2% and 95.8%, which also demonstrates the perfect localization of vortex wave in CMs. When the OAMs of the incident vortex wave are $l_{\text{in}} = -10$ or 10, the transmitted vortex wave with OAMs of 10 and −10 can be clearly observed outside the CMs, with transmissivity up to 94.3% and 93.1%, as depicted in Figs. 2(c) and 2(d), respectively. For the function of OAM selective conversion, the nature of this anomalous phenomenon is the reversal of reflected and transmitted diffraction order caused by multiple reflections in CMs. Specifically, when the vortex wave is incident with $l_{\text{in}} = -10$, the $\sigma = 1$ order is dominant in the transmission to cause a result of $l_t = 10$. When $l_{\text{in}} = 10$, the effective diffraction order is $\sigma = -1$, and the transmitted OAM is −10, which corresponds to the physical process analyzed in Fig. 1(b). In addition, CMs are not only effective for the manipulation of a single-vortex source, but also effective for multivortex sources. If only the selection function of vortex wave is required without OAM conversion, it can be achieved by placing additional metagratings of different sizes outside the CMs. (see Figs. S2 and S3 in Supplementary Material). In fact, these two different vortex wave manipulations are not limited to CMs with $m = 4$, but can be achieved for all cases with the even number of unit cells. Numerical demonstrations prove that the CMs with $m = 4$ can not only perfectly localize vortex waves, but also selectively convert a vortex wave with a specific OAM.

To further elucidate the working mechanism behind two multifunctional manipulations, we theoretically and numerically calculate the reflectivity and transmissivity of CMs with $m = 4$ at different diffraction orders with respect to the incident OAM. As depicted in Figs. 3(a) and 3(b), the analytical and numerical results are in good agreement, and the different diffraction orders play a crucial role in the transmission or reflection phenomena in CMs. When the incident OAM is in the range of −5 to 5, the reflectivity of $\sigma = 0$ order is almost 1, as indicated in Fig. 3(a). This means that the incident vortex source is completely reflected at $\sigma = 0$ order on the internal surface of CMs, i.e., $l_r = l_{\text{in}} + 0 \times q = l_{\text{in}}$. As the designed structure is completely enclosed, the reflected vortex will impinge on the internal surface for the second time as a new incident vortex source. As expected, the reflected vortex will still be perfectly reflected back, and continue to experience complete reflection inside the CMs. Finally, the vortex waves are completely confined within the CMs, which perfectly explains the observation of vortex fields

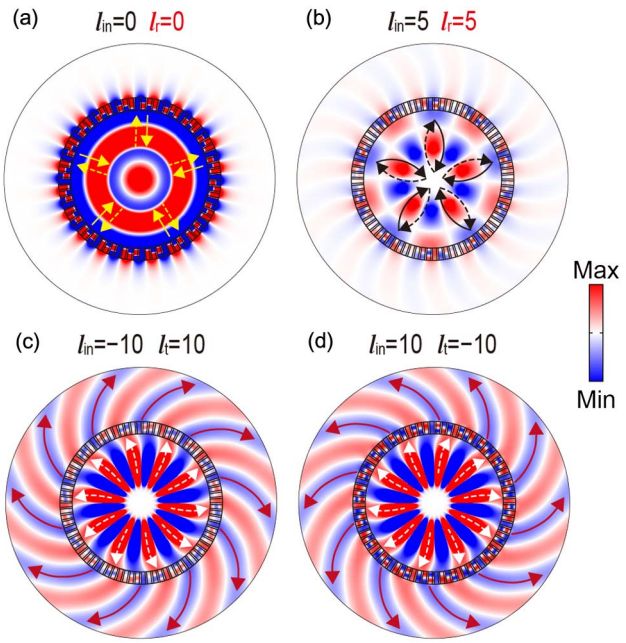

Fig. 2. Numerical demonstration for the multifunctional manipulation of vortex waves in CMs ($m = 4$) with $\gamma = 2$. The effect of vortex localization: (a) $l_{\text{in}} = 0$, $l_r = 0$ and (b) $l_{\text{in}} = 5$, $l_r = 5$. The function of OAM selective conversion: (c) $l_{\text{in}} = -10$, $l_t = 10$ and (d) $l_{\text{in}} = 10$, $l_t = -10$.

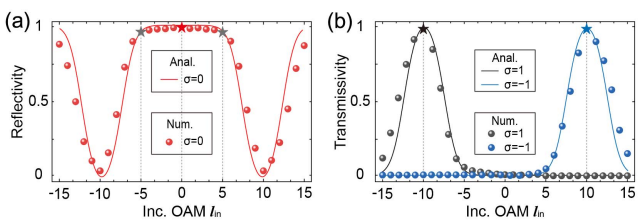

Fig. 3. Interpretation for two different vortex wave manipulations. The relationship between the relevant diffraction orders of (a) reflectivity, (b) transmissivity and the incident OAM l_{in} in CMs ($m = 4$) with $\gamma = 2$.

being only inside the structure in Figs. 2(a) and 2(b). In addition, when the OAM of an incident vortex equals −10, the transmissivity of $\sigma = 1$ order greatly exceeds that of the other diffraction orders, as indicated by the black pentagon in Fig. 3(b). Based on the proposed OAM conservation law [Eq. (1)], the OAM of the transmitted vortex is $l_t = l_{\text{in}} + 1 \times q = 10$, which corresponds to the result in Fig. 2(c). When $l_{\text{in}} = 10$, the transmissivity is dominated by the $\sigma = -1$ order [blue pentagon in Fig. 3(b)], and the transmitted OAM $l_t = l_{\text{in}} - 1 \times q = -10$, which also directly explains the numerical results in Fig. 2(d). The above analytical results illustrate that the transmission and reflection reversals of higher diffraction orders lead to the two different diffraction behaviors, and this effect is clear and robust.

Further explorations have proved that the CMs have a powerful ability to manipulate vortex waves for other parameters of q and γ. We comprehensively calculated CMs with $q = 15$, 20, and 25, and γ values from 1.5 to 3 to determine the critical values of OAM l_{crt} for vortex localization. The results in Fig. 4(a) show that with an increase in the q and γ, the maximum OAM value of vortex localization also nonlinearly increases, and the OAM obtained from Eq. (3) has an error that is negligible compared to the analytical results. Additionally, the simulation results in Fig. 4(a) are almost identical to the analytical results, which further confirms the validity of Eq. (3). For the function of OAM selective conversion, CMs overcomes the difficulty of selecting vortex wave with a specific OAM from a mixed vortex field (see Fig. S3 in Supplementary Material). Therefore, it is important to accurately determine the OAM of vortex selective conversion. Figure 4(b) clearly shows the variation rule of the selected OAM value with $\gamma = 2$ and the q changing from 15 to 25, which satisfies $|l_{\text{sle}}| \approx q/2$. It can be seen that the analytical results are slightly larger than the numerical results, which is caused by two factors. One is that the designed structure has a certain thickness, and the other is that the vortex source is located inside the CMs. In fact, when the vortex wave transmits from outside to inside of the CMs, the numerical simulation results are slightly larger than the analytical results, which is completely opposite to the results shown in Fig. 4(b). And when the thickness d is set to be much smaller than the wavelength, the numerical results are basically consistent with the analytical results. Therefore, we quantitatively confirm the critical OAM of vortex localization and the specific OAM value of vortex selective conversion.

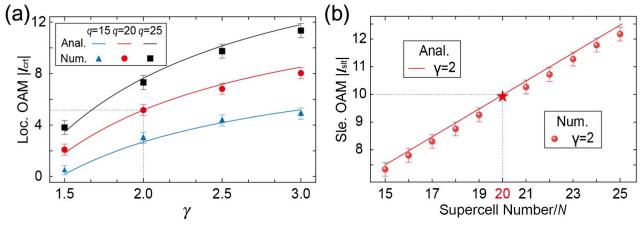

Fig. 4. The performance of vortex localization and OAM selective conversion in CMs with $m = 4$. (a) Relationship between the critical OAM of vortex localization $|l_{\text{crt}}|$ and different γ; (b) relationship between the OAM of vortex selective conversion $|l_{\text{slt}}|$ and supercell number N.

Finally, we would like to emphasize that two manipulation effects of vortex wave are highly robust, and present some relevant discussions. Specifically, when the even number of unit cells varies from 2 to 22, the designed CMs can achieve the same manipulation phenomenon of vortex waves, i.e., the same $|l_{\text{crt}}|$ and $|l_{\text{slt}}|$ (see Figs. S4 and S5 in Supplementary Material). Notably, due to the reversal of the parity-dependent transmission and reflection, the important function of vortex manipulation described above is only available for m of even numbers, and not for the case of odd m (see Fig. S5 in Supplementary Material; the details with $m = 3$ are shown as well). In addition, the CMs also show wideband response properties and can accommodate the off-center of vortex sources. The results indicate that when the wavelength variation range is less than 0.25λ and the off-center distance of vortex source is less than 0.2λ, the CMs can still effectively localize and selectively convert vortex waves (see Figs. S7 and S8 in Supplementary Material).

3. Conclusion

In summary, we propose a new theory that can realize the multifunctional manipulation of arbitrary vortex waves in CMs (m is even). The theoretical and numerical results indicate that the periodic phase structure provides an additional topological charge and makes the reflected and transmitted OAMs satisfy a new OAM conservation law. Furthermore, we quantitatively determine the OAM range of vortex localization, as well as the specific OAM values of vortex wave selective conversion. The analytical results clearly demonstrate that CMs can achieve perfect manipulation of vortex waves by reversing the reflectivity and transmissivity through different diffraction orders. Finally, we explore the performance stability and multifunctional applications of the designed structure. Overall, this research provides important references for designing OAM-based devices and has broad application prospects in the field of vortex manipulation.

Acknowledgements

This work was supported by the National Natural Science Foundation of China (Nos. 92050102, 11974010, and 12274313), the Fundamental Research Funds for the Central Universities (Nos. 20720230102 and 20720220033), the National Key R & D Program of China (Nos. 2020YFA0710100, 2022YFA1404400, and 2022YFA1404300), and the China Scholarship Council (No. 202106310002).

References

1. Z. H. Jiang and D. H. Werner, *Electromagnetic Vortices: Wave Phenomena and Engineering Applications* (John Wiley & Sons, 2021).
2. Y. Shen, X. Wang, Z. Xie, *et al.*, "Optical vortices 30 years on: OAM manipulation from topological charge to multiple singularities," Light Sci. Appl. **8**, 90 (2019).

3. P. Coullet, L. Gil, and F. Rocca, "Optical vortices," Opt. Commun. **73**, 403 (1989).
4. S. M. Barnett and L. Allen, "Orbital angular momentum and nonparaxial light beams," Opt. Commun. **110**, 670 (1994).
5. M. V. Berry, "A note on superoscillations associated with Bessel beams," J. Opt. **15**, 044006 (2013).
6. M. V. Berry and W. Liu, "No general relation between phase vortices and orbital angular momentum," J. Phys. A: Math. Theor. **55**, 374001 (2022).
7. C.-W. Qiu and Y. Yang, "Vortex generation reaches a new plateau," Science **357**, 645 (2017).
8. X. Jiang, Y. Li, B. Liang, *et al.*, "Convert acoustic resonances to orbital angular momentum," Phys. Rev. Lett. **117**, 034301 (2016).
9. L. Yan, P. Gregg, E. Karimi, *et al.*, "Q-plate enabled spectrally diverse orbital-angular-momentum conversion for stimulated emission depletion microscopy," Optica **2**, 900 (2015).
10. Z. Hu, N. He, Y. Sun, *et al.*, "Wideband high-reflection chiral dielectric metasurface," Prog. Electromagn. Res. **172**, 51 (2021).
11. Z. Hao, Y. Zhou, B. Wu, *et al.*, "Improving resolution of superlens based on solid immersion mechanism," Chin. Phys. B **32**, 064211 (2023).
12. X. Fang, H. Ren, and M. Gu, "Orbital angular momentum holography for high-security encryption," Nat. Photonics **14**, 102 (2020).
13. H. Ren, X. Fang, J. Jang, *et al.*, "Complex-amplitude metasurface-based orbital angular momentum holography in momentum space," Nat. Nanotechnol. **15**, 948 (2020).
14. A. Mair, A. Vaziri, G. Weihs, *et al.*, "Entanglement of the orbital angular momentum states of photons," Nature **412**, 313 (2001).
15. J. Leach, B. Jack, J. Romero, *et al.*, "Quantum correlations in optical angle–orbital angular momentum variables," Science **329**, 662 (2010).
16. H. Chen, C. T. Chan, and P. Sheng, "Transformation optics and metamaterials," Nat. Mater. **9**, 387 (2010).
17. J. Yim, N. Chandra, X. Feng, *et al.*, "Broadband continuous supersymmetric transformation: a new paradigm for transformation optics," eLight **2**, 16 (2022).
18. Z. Hao, Y. Zhuang, Y. Chen, *et al.*, "Effective medium theory of checkboard structures in the long-wavelength limit," Chin. Opt. Lett. **18**, 072401 (2020).
19. Y. Fu, C. Shen, X. Zhu, *et al.*, "Sound vortex diffraction via topological charge in phase gradient metagratings," Sci. Adv. **6**, eaba9876 (2020).
20. Z. Zou, R. Lirette, and L. Zhang, "Orbital angular momentum reversal and asymmetry in acoustic vortex beam reflection," Phys. Rev. Lett. **125**, 074301 (2020).
21. H.-F. Huang and H.-M. Huang, "Millimeter-wave wideband high efficiency circular airy OAM multibeams with multiplexing OAM modes based on transmission metasurfaces," Prog. Electromagn. Res. **173**, 151 (2022).
22. X. Cai, J. Wang, M. J. Strain, *et al.*, "Integrated compact optical vortex beam emitters," Science **338**, 363 (2012).
23. Z. Shao, J. Zhu, Y. Chen, *et al.*, "Spin-orbit interaction of light induced by transverse spin angular momentum engineering," Nat. Commun. **9**, 926 (2018).
24. Y. Li, X. Li, L. Chen, *et al.*, "Orbital angular momentum multiplexing and demultiplexing by a single metasurface," Adv. Opt. Mater. **5**, 1600502 (2017).
25. R. C. Devlin, A. Ambrosio, N. A. Rubin, *et al.*, "Arbitrary spin-to-orbital angular momentum conversion of light," Science **358**, 896 (2017).
26. Y. Xu, Y. Fu, and H. Chen, "Steering light by a sub-wavelength metallic grating from transformation optics," Sci. Rep. **5**, 12219 (2015).
27. Y. Xu, Y. Fu, and H. Chen, "Planar gradient metamaterials," Nat. Rev. Mater. **1**, 16067 (2016).
28. Y. Fu, C. Shen, Y. Cao, *et al.*, "Reversal of transmission and reflection based on acoustic metagratings with integer parity design," Nat. Commun. **10**, 2326 (2019).
29. Y. Ra'di, D. L. Sounas, and A. Alu, "Metagratings: beyond the limits of graded metasurfaces for wave front control," Phys. Rev. Lett. **119**, 067404 (2017).
30. Y. Cao, Y. Fu, Q. Zhou, *et al.*, "Mechanism behind angularly asymmetric diffraction in phase-gradient metasurfaces," Phys. Rev. Appl. **12**, 024006 (2019).
31. Y. Fu, Y. Tian, X. Li, *et al.*, "Asymmetric generation of acoustic vortex using dual-layer metasurfaces," Phys. Rev. Lett. **128**, 104501 (2022).
32. Z. Hao, H. Chen, Y. Yin, *et al.*, "Asymmetric conversion of arbitrary vortex fields via acoustic metasurface," Appl. Phys. Lett. **123**, 201702 (2023).
33. A. Arbabi, E. Arbabi, Y. Horie, *et al.*, "Planar metasurface retroreflector," Nat. Photonics **11**, 415 (2017).
34. W. Luo, S. Xiao, Q. He, *et al.*, "Photonic spin Hall effect with nearly 100% efficiency," Adv. Opt. Mater. **3**, 1102 (2015).
35. X.-D. Fan and L. Zhang, "Acoustic orbital angular momentum Hall effect and realization using a metasurface," Phys. Rev. Res. **3**, 013251 (2021).
36. Z. Zhang, M. Kang, X. Zhang, *et al.*, "Coherent perfect diffraction in metagratings," Adv. Mater. **32**, 2002341 (2020).
37. G. Ma, M. Yang, S. Xiao, *et al.*, "Acoustic metasurface with hybrid resonances," Nat. Mater. **13**, 873 (2014).
38. L. Li, H. Zhao, C. Liu, *et al.*, "Intelligent metasurfaces: control, communication and computing," eLight **2**, 7 (2022).
39. Y. Yang, L. Wu, Y. Liu, *et al.*, "Deuterogenic plasmonic vortices," Nano Lett. **20**, 6774 (2020).
40. Y. Ming, W. Zhang, J. Tang, *et al.*, "Nonlinear wavy metasurfaces with topological defects for manipulating orbital angular momentum states," ACS Photonics **8**, 1896 (2021).
41. T. Liu, S. An, Z. Gu, *et al.*, "Chirality-switchable acoustic vortex emission via non-Hermitian selective excitation at an exceptional point," Sci. Bull. **67**, 1131 (2022).
42. Y. Cao, Y. Fu, J.-H. Jiang, *et al.*, "Scattering of light with orbital angular momentum from a metallic meta-cylinder with engineered topological charge," ACS Photonics **8**, 2027 (2021).
43. J. Li, A. Díaz-Rubio, C. Shen, *et al.*, "Highly efficient generation of angular momentum with cylindrical bianisotropic metasurfaces," Phys. Rev. Appl. **11**, 024016 (2019).
44. D. Lee, S. So, G. Hu, *et al.*, "Hyperbolic metamaterials: fusing artificial structures to natural 2D materials," eLight **2**, 1 (2022).
45. Z. Li, G. Cao, C. Li, *et al.*, "Non-Hermitian electromagnetic metasurfaces at exceptional points," Prog. Electromagn. Res. **171**, 1 (2021).
46. A. Mirzaei, A. E. Miroshnichenko, I. V. Shadrivov, *et al.*, "Optical metacages," Phys. Rev. Lett. **115**, 215501 (2015).
47. C. Liu, J. Shi, W. Zhao, *et al.*, "Three-dimensional soundproof acoustic metacage," Phys. Rev. Lett. **127**, 084301 (2021).